Semnan University

Mechanics of Advanced Composite Structures

journal homepage: http://MACS.journals.semnan.ac.ir

# Numerical Investigation on Thermal Post-buckling Of Annular Sector Plates Made of FGM Via 3D Finite Element Method

**M. Shahsavari[a], K. Asemi [a*], M. Babaei[b], F. Kiarasi[b],**

[a]*Mechanical Engineering Department, Islamic Azad University, Tehran North Branch, Tehran, Iran*
[b]*Mechanical Engineering Department, University of Eyvanakey, Semnan, Iran*

**KEYWORDS**

Thermal post-buckling analysis
3D elasticity
FGM annular sector plate
Finite element method

**ABSTRACT**

This paper presents the thermal post-buckling analysis of functionally graded annular sector plates subjected to uniform temperature rise for the first time. The plate is consisting of a composed ceramic-metal material which the volume fraction of the component materials is assumed to change continuously through the thickness via a simple power law distribution.3D elasticity theory and non-linear Green strain tensor are used to derive the governing equations which are extended based on the principle of virtual work and solved via the graded finite element method. The non-linear equilibrium equations are solved by applying the Newton–Raphson procedure. The influences of material gradient exponent, various sector angles, thickness ratio, aspect ratio on the thermal post-buckling response of FGM annular sector plates subjected to uniform temperature rise are presented. Results indicate that the thermal post-buckling response of FGM annular sector plates can be considered as a bifurcation point following a stable post-buckling path.

## 1. Introduction

In recent years, functionally graded materials (FGMs) as a kind of thermal barrier materials have been used for structural components subjected to exceedingly high-temperature environments including nuclear reactors and high-speed spacecraft industries. In such conditions, high-temperature which is induced compressive stresses will be developed in the constrained plates; therefore, it will lead to buckling. Annular sector plates are often used as structural components in many engineering applications and are subjected to different thermal loading conditions. Hence, the thermal buckling and post-buckling response of FGM annular sector plates are of incited interest for engineering design. Gas turbine rotating blades made of FGMs can be considered as one of the applications of FGM annular sector plates subjected to high thermal loadings.

Although many researches have been conducted on the thermal buckling [1-6] and post-buckling [7-17] analysis of rectangular FG plates and beams, among the plate-type structures, there has been less research attention on thermal buckling [18-25] and post-buckling analysis [26-32] of FGM circular and annular plate. There are a few studies related to buckling and post-buckling of FGM annular sector plates under mechanical load. For instance, based on classical plate theory, Hosseini-Hashemi et al. [33] performed DQ analysis for buckling behavior of radially FG circular and annular sector plates witch located on the Pasternak elastic foundation. Based on FSDT theory, Naderi and Saidi [34-36] employed an analytical solution to investigate the buckling behavior of relatively thick FG annular and sector plates located on the Winkler elastic foundation. Asemi et al. applied 3D elasticity and finite element method to study biaxial [37] and shear [38] buckling analysis of FGM annular sector plates resting on Winkler elastic foundation with fully or partially supported boundary conditions. Also, limited investigation focused on the thermal buckling of FGM annular sector plate, for example, Saidi and Baferani [39] investigated thermal buckling analysis of relatively thick FG annular sector plates. The equilibrium and stability equations are obtained

* Corresponding author. Tel.: +98-9122484921 ; Fax: +98-21-77009848
*E-mail address:* k.asemi@iau-tnb.ac.ir

DOI: 10.22075/MACS.2021.21158.1293
Received 20-08-20; Received in revised form 20-12-13; Accepted 21-04-01

based on FSDT. Finally, an analytical method was applied to solve it. In another study, Jabbarrzadeh et al [40] utilized FSDT and Von Karman's assumptions to study the thermal buckling of FG annular sector plate. Differential quadrature method was applied to solve the equilibrium and stability equations. Based on FSDT, Shaterzadeh and his co-authors investigated thermal buckling analysis of symmetric and anti-symmetric laminated composite plates with a cut-out [41], and thermo-mechanical buckling analysis of FGM plates with an elliptic cutout [42]. In addition, Shaterzadeh et al [43] applied FSDT and finite element method to study the thermal buckling analysis of perforated FGM plates. 3D thermomechanical buckling analysis of perforated annular sector plates with multiaxial material heterogeneities based on curved B-spline elements was presented by Shariyat et al [44]. Based on 3D elasticity and Green's nonlinear strain assumptions, Behzad et al [45] carried out the investigation about the thermal buckling analysis of FG perforated annular sector plates. Shaterzadeh et al [46] studied the stability analysis of FG annular sector plate under thermomechanical loading via 3D elasticity theory and using finite element method.

From the above literature review, it can be seen that the nonlinear Von Karman's assumptions and plate theories have been mostly applied to investigate post-buckling analysis of functionally graded material plates. In this paper, 3D elasticity theory and green's assumptions are employed. 3D elasticity leads to more realistic and accurate results than the other plate theories. Furthermore, the complete Green strain tensor is more acceptable for analyzing the geometrically non-linear behavior of the plates.

In this work, a numerical method is carried out by using the nonlinear Green strain tensor and, FEM based on 3D-elasticity theory to study the thermal post-buckling of FGM annular sector plates subjected to uniform temperature rise. The plate is consisting of a composed ceramic-metal material which the volume fraction of the component materials is assumed to change continuously through the thickness via a simple power law distribution. Three various boundary conditions have been considered such as: 1- Immovable simply supported edges. 2- Immovable simply supported radial edges and free circumferential edges. 3- Immovable simply supported circumferential edges and free radial edges. The principle of virtual work is utilized to derive the governing equations and the iterative Newton–Raphson procedure is applied to solve the non-linear equilibrium equations. The impact of material gradient index, sector angle, aspect ratio, and thickness ratio on the thermal post-buckling behavior of FGM annular sector plates have been examined. The novel point of this paper is the investigation of thermal post-buckling behaviour of FGM annular sector plate with considering various boundary conditions for the first time.

## 2. Materials Properties and Geometry

A cermet FGM annular sector plate is considered. $h$, $a$, $b$ and $\beta$ are thickness, inner and outer radius of the sector, respectively. The geometry of the problem $\left(a \le r \le b.\ \frac{-\beta}{2} \le \theta \le \frac{\beta}{2}.\ 0 \le z \le h\right)$ are shown in Fig. 1.

The material properties of the FGM annular sector plate across the thickness are defined as follows:

$$Q = Q_m + (Q_c - Q_m)\left(\frac{z}{h}\right)^n \tag{1}$$

in which Q indicates material property including modulus of elasticity and coefficient of thermal expansion $\alpha$, and subscripts m and c related to the metal and ceramic component, respectively. Poisson's ratio is considered to be constant along with the thickness.

## 3. 3D Elasticity Theory

Hooke's law for this structure is considered as:

$$\sigma = D(\varepsilon - \varepsilon^{Th}) \tag{2}$$

where:

$$\begin{aligned} \sigma &= [\sigma_{rr}, \sigma_{\theta\theta}, \sigma_{zz}, \sigma_{r\theta}, \sigma_{\theta z}, \sigma_{rz}]^T \\ \varepsilon &= [\varepsilon_{rr}, \varepsilon_{\theta\theta}, \varepsilon_{zz}, 2\varepsilon_{r\theta}, 2\varepsilon_{\theta z}, 2\varepsilon_{rz}]^T \\ \varepsilon^{Th} &= [\alpha\Delta T, \alpha\Delta T, \alpha\Delta T, 0,0,0]^T \end{aligned} \tag{3}$$

where $\varepsilon_{ij}^{Th}$ is the thermal strain components and $\sigma_{ij}$ and $\varepsilon_{ij}(i.j = r.\theta.z)$ are the stress and strain tensor components in cylindrical coordinates, respectively, and the elasticity matrix D is as:

$$\boldsymbol{D} = \frac{E(z)(1-\nu)}{(1+\nu)(1-2\nu)} \begin{pmatrix} 1 & \frac{\nu}{1-\nu} & \frac{\nu}{1-\nu} & 0 & 0 & 0 \\ \frac{\nu}{1-\nu} & 1 & \frac{\nu}{1-\nu} & 0 & 0 & 0 \\ \frac{\nu}{1-\nu} & \frac{\nu}{1-\nu} & 1 & 0 & 0 & 0 \\ 0 & 0 & 0 & \frac{1-2\nu}{2(1-\nu)} & 0 & 0 \\ 0 & 0 & 0 & 0 & \frac{1-2\nu}{2(1-\nu)} & 0 \\ 0 & 0 & 0 & 0 & 0 & \frac{1-2\nu}{2(1-\nu)} \end{pmatrix} = E(z)\Phi \tag{4}$$

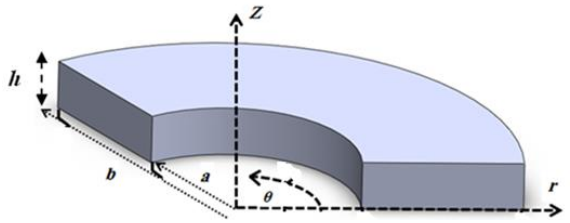


**Fig. 1.** Geometry of annular sector plate

It is assumed that the elasticity modulus E varies along the thickness direction whereas Poisson's ratio ν is assumed to be constant. Therefore Matrix ϕ is constant.

The Green strain displacement relations in cylindrical coordinates are assumed as follows:

$$\varepsilon = \varepsilon_L + \varepsilon_{NL} \tag{5}$$

$$\varepsilon_L = \begin{Bmatrix} \frac{\partial u}{\partial r} \\ \frac{u + \frac{\partial v}{\partial \theta}}{r} \\ \frac{\partial w}{\partial z} \\ \frac{\frac{\partial u}{\partial \theta} - v}{r} + \frac{\partial v}{\partial r} \\ \frac{\partial v}{\partial z} + \frac{\partial w}{r\,\partial \theta} \\ \frac{\partial u}{\partial z} + \frac{\partial w}{\partial r} \end{Bmatrix}, \quad \varepsilon_{NL} = \begin{Bmatrix} \frac{1}{2}\left(\left(\frac{\partial u}{\partial r}\right)^2 + \left(\frac{\partial v}{\partial r}\right)^2 + \left(\frac{\partial w}{\partial r}\right)^2\right) \\ \frac{1}{2}\left(\left(\frac{\frac{\partial u}{\partial \theta} - v}{r}\right)^2 + \left(\frac{\frac{\partial v}{\partial \theta} + u}{r}\right)^2 + \left(\frac{\frac{\partial w}{\partial \theta}}{r}\right)^2\right) \\ \frac{1}{2}\left(\left(\frac{\partial u}{\partial z}\right)^2 + \left(\frac{\partial v}{\partial z}\right)^2 + \left(\frac{\partial w}{\partial z}\right)^2\right) \\ \frac{\partial u}{\partial r}\frac{\frac{\partial u}{\partial \theta} - v}{r} + \frac{\partial v}{\partial r}\frac{\frac{\partial v}{\partial \theta} + u}{r} + \frac{\partial w}{\partial r}\frac{\partial w}{r\,\partial \theta} \\ \frac{\partial u}{\partial \theta} - v}{r}\frac{\partial u}{\partial z} + \frac{\frac{\partial v}{\partial \theta} + u}{r}\frac{\partial v}{\partial z} + \frac{\partial w}{\partial z}\frac{\partial w}{r\,\partial \theta} \\ \frac{\partial u}{\partial z}\frac{\partial u}{\partial r} + \frac{\partial v}{\partial z}\frac{\partial v}{\partial r} + \frac{\partial w}{\partial z}\frac{\partial w}{\partial r} \end{Bmatrix} \tag{6}$$

The cylindrical and natural coordinates are defined by

$$\xi = \frac{(2r - a^{(e)} - b^{(e)})}{(b^{(e)} - a^{(e)})}, \quad \eta = \frac{2(\theta - \theta_c)}{\beta^{(e)}}, \quad \zeta = \frac{2(z - z_c)}{h^{(e)}} \tag{7}$$

where $-1 \le \xi.\ \eta.\zeta \le 1$ are through r, θ and z coordinate axes, respectively. $a^{(e)}.b^{(e)}.\beta^{(e)}$ *and* $h^{(e)}$ are the inner radius, outer radius, sector angle, and thickness of each annular sector element.

Hence, the linear part of strain-displacement relations (6) can be considered in matrix form in terms of cylindrical coordinate system as:

$$\varepsilon_L = d_L \mathbb{Q} \tag{8}$$

where the linear part of strain-displacement relations based on natural coordinates can be expressed as:

$$\varepsilon_L = \Gamma \mathbb{Q} \tag{9}$$

$$\Gamma = \begin{bmatrix} \frac{\partial}{\partial \xi}\frac{2}{b^{(e)} - a^{(e)}} & 0 & 0 \\ \frac{2}{\xi\left(b^{(e)} - a^{(e)}\right) + a^{(e)} + b^{(e)}} & \frac{4}{\xi\left(b^{(e)} - a^{(e)}\right) + a^{(e)} + b^{(e)}}\frac{\partial}{\beta^{(e)}\partial \eta} & 0 \\ 0 & 0 & \frac{2\partial}{h^{(e)}\partial \zeta} \\ \frac{4}{\xi\left(b^{(e)} - a^{(e)}\right) + a^{(e)} + b^{(e)}}\frac{\partial}{\beta^{(e)}\partial \eta} & \frac{\partial}{\partial \xi}\frac{2}{b^{(e)} - a^{(e)}} - \frac{2}{\xi\left(b^{(e)} - a^{(e)}\right) + a^{(e)} + b^{(e)}} & 0 \\ 0 & \frac{2\partial}{h^{(e)}\partial \zeta} & \frac{4}{\xi\left(b^{(e)} - a^{(e)}\right) + a^{(e)} + b^{(e)}}\frac{\partial}{\beta^{(e)}\partial \eta} \\ \frac{2\partial}{h^{(e)}\partial \zeta} & 0 & \frac{\partial}{\partial \xi}\frac{2}{b^{(e)} - a^{(e)}} \end{bmatrix} \tag{10}$$

Consider the three-dimensional 8-node linear brick element (Fig. 2-b). In comparison to the conventional brick elements, material properties are among the nodal degrees of freedom. The displacement field vector $\mathbb{Q}$ of an optional point of the element may be related to the nodal displacement vectors of the element $\Delta^{(e)}$ through the shape function matrix N, as:

$$\mathbb{Q} = \boldsymbol{N}\Delta^{(e)} \tag{11}$$

where:

$$\Delta^{(e)} = \{U_1 \;\; V_1 \;\; W_1 \;\; . \;\; . \;\; . \;\; U_8 \;\; V_8 \;\; W_8\}^{\mathbf{T}} \tag{12}$$

$$\boldsymbol{N} = \begin{bmatrix} N_1 & 0 & 0 & N_2 & 0 & 0 & \dots & N_8 & 0 & 0 \\ 0 & N_1 & 0 & 0 & N_2 & 0 & \dots & 0 & N_8 & 0 \\ 0 & 0 & N_1 & 0 & 0 & N_2 & \dots & 0 & 0 & N_8 \end{bmatrix}_{3*24} \tag{13}$$

Matrix N based on the natural coordinates can be expressed as [47]:

$$N_i(\xi, \eta, \zeta) = \frac{1}{8}(1 + \xi_i\xi)(1 + \eta_i\eta)(1 + \zeta_i\zeta) \tag{14}$$

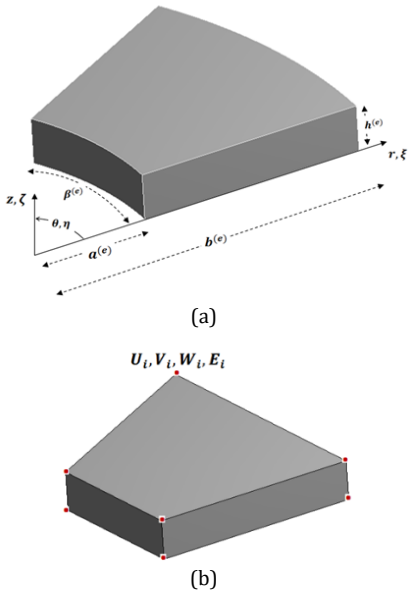


**Fig. 2.** Schematic of an annular sector element.

Replacing (11) into (8), the linear part of strain-displacement can be expressed as:

$$\varepsilon_L^{(e)} = \boldsymbol{d}_L \boldsymbol{N} \Delta^{(e)} = \boldsymbol{B}_L \Delta^{(e)} \tag{15}$$

where:

$$\boldsymbol{B}_L = \begin{pmatrix} \frac{\partial N_1}{\partial r} & 0 & 0 & \frac{\partial N_2}{\partial r} & 0 & 0 & \dots & \frac{\partial N_8}{\partial r} & 0 & 0 \\ \frac{N_1}{r} & \frac{\partial N_1}{r\partial\theta} & 0 & \frac{N_2}{r} & \frac{\partial N_2}{r\partial\theta} & 0 & \dots & \frac{N_8}{r} & \frac{\partial N_8}{r\partial\theta} & 0 \\ 0 & 0 & \frac{\partial N_1}{\partial z} & 0 & 0 & \frac{\partial N_2}{\partial z} & \dots & 0 & 0 & \frac{\partial N_8}{\partial z} \\ \frac{\partial N_1}{r\partial\theta} & \frac{\partial N_1}{\partial r} - \frac{N_1}{r} & 0 & \frac{\partial N_2}{r\partial\theta} & \frac{\partial N_2}{\partial r} - \frac{N_2}{r} & 0 & \dots & 0 & \frac{\partial N_8}{r\partial\theta} & \frac{\partial N_8}{\partial r} - \frac{N_8}{r} \\ 0 & \frac{\partial N_1}{\partial z} & \frac{\partial N_1}{r\partial\theta} & 0 & \frac{\partial N_2}{\partial z} & \frac{\partial N_2}{r\partial\theta} & \dots & 0 & \frac{\partial N_8}{\partial z} & \frac{\partial N_8}{r\partial\theta} \\ \frac{\partial N_1}{\partial z} & 0 & \frac{\partial N_1}{\partial r} & \frac{\partial N_2}{\partial z} & 0 & \frac{\partial N_2}{\partial r} & \dots & \frac{\partial N_8}{\partial z} & 0 & \frac{\partial N_8}{\partial r} \end{pmatrix}_{6*24} \tag{16}$$

Moreover, by substituting (11) into (9), the linear part of strain-displacement relations in terms of natural coordinate system can be expressed as:

$$\varepsilon_L^{(e)} = \Gamma \boldsymbol{N} \Delta^{(e)} = \mathcal{B}_L \Delta^{(e)} \tag{17}$$

where $B_L^{(i)} . j = 1.2 \dots .8$ are:

$$\mathcal{B}_L = \begin{pmatrix} \mathcal{B}_L^{(1)} & \mathcal{B}_L^{(2)} & \mathcal{B}_L^{(3)} & \mathcal{B}_L^{(4)} & \mathcal{B}_L^{(5)} & \mathcal{B}_L^{(6)} & \mathcal{B}_L^{(7)} & \mathcal{B}_L^{(8)} \end{pmatrix} \tag{18}$$

$$\begin{aligned}
\mathcal{B}_L^i(1,:) &= \begin{pmatrix} \frac{\xi_i(1+\eta_i\eta)(1+\zeta_i\zeta)}{4\left(b^{(e)}-a^{(e)}\right)} & 0 & 0 \end{pmatrix} \\
\mathcal{B}_L^i(2,:) &= \begin{pmatrix} \frac{(1+\xi_i\xi)(1+\eta_i\eta)(1+\zeta_i\zeta)}{4\left(\xi\left(b^{(e)}-a^{(e)}\right)+a^{(e)}+b^{(e)}\right)} & \frac{\eta_i(1+\xi_i\xi)(1+\zeta_i\zeta)}{2\beta^{(e)}\left(\xi\left(b^{(e)}-a^{(e)}\right)+a^{(e)}+b^{(e)}\right)} & 0 \end{pmatrix} \\
\mathcal{B}_L^i(3,:) &= \begin{pmatrix} 0 & 0 & \frac{\zeta_i(1+\xi_i\xi)(1+\eta_i\eta)}{4h^{(e)}} \end{pmatrix} \\
\mathcal{B}_L^i(4,:) &= \begin{pmatrix} \frac{\eta_i(1+\xi_i\xi)(1+\zeta_i\zeta)}{2\beta^{(e)}\left(\xi\left(b^{(e)}-a^{(e)}\right)+a^{(e)}+b^{(e)}\right)} & \frac{\xi_i(1+\eta_i\eta)(1+\zeta_i\zeta)}{4\left(b^{(e)}-a^{(e)}\right)} - \frac{(1+\xi_i\xi)(1+\eta_i\eta)(1+\zeta_i\zeta)}{4\left(\xi\left(b^{(e)}-a^{(e)}\right)+a^{(e)}+b^{(e)}\right)} & 0 \end{pmatrix} \\
\mathcal{B}_L^i(5,:) &= \begin{pmatrix} 0 & \frac{\zeta_i(1+\xi_i\xi)(1+\eta_i\eta)}{4h^{(e)}} & \frac{\eta_i(1+\xi_i\xi)(1+\zeta_i\zeta)}{2\beta^{(e)}\left(\xi\left(b^{(e)}-a^{(e)}\right)+a^{(e)}+b^{(e)}\right)} \end{pmatrix} \\
\mathcal{B}_L^i(6,:) &= \begin{pmatrix} \frac{\zeta_i(1+\xi_i\xi)(1+\eta_i\eta)}{4h^{(e)}} & 0 & \frac{\xi_i(1+\eta_i\eta)(1+\zeta_i\zeta)}{4\left(b^{(e)}-a^{(e)}\right)} \end{pmatrix}
\end{aligned} \tag{19}$$

The non-linear part of strain-displacement relations in terms of cylindrical coordinate system can be considered as:

$$\varepsilon_{NL}^{(e)} = \boldsymbol{B}_{NL} \Delta^{(e)} \tag{20}$$

where:

$$\boldsymbol{B}_{NL} = \begin{pmatrix} \boldsymbol{B}_{NL}^{(1)} & \boldsymbol{B}_{NL}^{(2)} & \boldsymbol{B}_{NL}^{(3)} & \boldsymbol{B}_{NL}^{(4)} & \boldsymbol{B}_{NL}^{(5)} & \boldsymbol{B}_{NL}^{(6)} & \boldsymbol{B}_{NL}^{(7)} & \boldsymbol{B}_{NL}^{(8)} \end{pmatrix} \tag{21}$$

in which $B_{NL}^{(j)} . j = 1.2 \dots .8$ are as following sub-matrices.

$$\begin{aligned}
\boldsymbol{B}_{NL}^{(j)}(1,:) &= \left[ \frac{1}{2}\frac{\partial N_j}{\partial r} \sum_{i=1}^{8}\left(\frac{\partial N_i}{\partial r}U_i\right) \;\; \frac{1}{2}\frac{\partial N_j}{\partial r} \sum_{i=1}^{8}\left(\frac{\partial N_i}{\partial r}V_i\right) \;\; \frac{1}{2}\frac{\partial N_j}{\partial r} \sum_{i=1}^{8}\left(\frac{\partial N_i}{\partial r}W_i\right) \right] \\
\boldsymbol{B}_{NL}^{(j)}(2,1) &= \frac{1}{2}\left( \frac{\partial N_j}{r\partial\theta}\left( \sum_{i=1}^{8}\left(\frac{\partial N_i}{r\partial\theta}U_i\right) - 2\sum_{i=1}^{8}\left(\frac{N_i}{r}V_i\right) \right) + \frac{N_j}{r}\sum_{i=1}^{8}\left(\frac{N_i}{r}U_i\right) \right) \\
\boldsymbol{B}_{NL}^{(j)}(2,2) &= \frac{1}{2}\left( \frac{\partial N_j}{r\partial\theta}\left( \sum_{i=1}^{8}\left(\frac{\partial N_i}{r\partial\theta}V_i\right) + 2\sum_{i=1}^{8}\left(\frac{N_i}{r}U_i\right) \right) + \frac{N_j}{r}\sum_{i=1}^{8}\left(\frac{N_i}{r}V_i\right) \right)
\end{aligned} \tag{21}$$

$$\begin{aligned}
\boldsymbol{B}_{NL}^{(j)}(2,3) &= \frac{1}{2}\frac{\partial N_j}{r\partial\theta}\sum_{i=1}^{8}\left(\frac{\partial N_i}{r\partial\theta}W_i\right) \\
\boldsymbol{B}_{NL}^{(j)}(3,:) &= \left[ \frac{1}{2}\frac{\partial N_j}{\partial z}\sum_{i=1}^{8}\left(\frac{\partial N_i}{\partial z}U_i\right) \;\; \frac{1}{2}\frac{\partial N_j}{\partial z}\sum_{i=1}^{8}\left(\frac{\partial N_i}{\partial z}V_i\right) \;\; \frac{1}{2}\frac{\partial N_j}{\partial z}\sum_{i=1}^{8}\left(\frac{\partial N_i}{\partial z}W_i\right) \right] \\
\boldsymbol{B}_{NL}^{(j)}(4,1) &= \frac{\partial N_j}{\partial r}\left( \sum_{i=1}^{8}\left(\frac{\partial N_i}{r\partial\theta}U_i\right) - \sum_{i=1}^{8}\left(\frac{N_i}{r}V_i\right) \right) \\
\boldsymbol{B}_{NL}^{(j)}(4,2) &= \frac{\partial N_j}{\partial r}\left( \sum_{i=1}^{8}\left(\frac{\partial N_i}{r\partial\theta}V_i\right) + \sum_{i=1}^{8}\left(\frac{N_i}{r}U_i\right) \right) \\
\boldsymbol{B}_{NL}^{(j)}(4,3) &= \frac{\partial N_j}{\partial r}\sum_{i=1}^{8}\left(\frac{\partial N_i}{r\partial\theta}W_i\right) \\
\boldsymbol{B}_{NL}^{(j)}(5,1) &= \frac{\partial N_j}{\partial z}\left( \sum_{i=1}^{8}\left(\frac{\partial N_i}{r\partial\theta}U_i\right) - \sum_{i=1}^{8}\left(\frac{N_i}{r}V_i\right) \right) \\
\boldsymbol{B}_{NL}^{(j)}(5,2) &= \frac{\partial N_j}{\partial z}\left( \sum_{i=1}^{8}\left(\frac{\partial N_i}{r\partial\theta}V_i\right) + \sum_{i=1}^{8}\left(\frac{N_i}{r}U_i\right) \right) \\
\boldsymbol{B}_{NL}^{(j)}(5,3) &= \frac{\partial N_j}{\partial z}\sum_{i=1}^{8}\left(\frac{\partial N_i}{r\partial\theta}W_i\right) \\
\boldsymbol{B}_{NL}^{(j)}(6,:) &= \left[ \frac{\partial N_j}{\partial r}\sum_{i=1}^{8}\left(\frac{\partial N_i}{\partial z}U_i\right) \;\; \frac{\partial N_j}{\partial r}\sum_{i=1}^{8}\left(\frac{\partial N_i}{\partial z}V_i\right) \;\; \frac{\partial N_j}{\partial r}\sum_{i=1}^{8}\left(\frac{\partial N_i}{\partial z}W_i\right) \right]
\end{aligned} \tag{22}$$

Also, the non-linear part of strain-displacement relations in terms of natural coordinates is as:

$$\varepsilon_{NL}^{(e)} = \mathcal{B}_{NL} \Delta^{(e)} \tag{23}$$

where:

$$\mathcal{B}_{NL} = \begin{pmatrix} \mathcal{B}_{NL}^{(1)} & \mathcal{B}_{NL}^{(2)} & \mathcal{B}_{NL}^{(3)} & \mathcal{B}_{NL}^{(4)} & \mathcal{B}_{NL}^{(5)} & \mathcal{B}_{NL}^{(6)} & \mathcal{B}_{NL}^{(7)} & \mathcal{B}_{NL}^{(8)} \end{pmatrix} \tag{24}$$

where $B_{NL}^{(j)} . j = 1.2 \dots .8$ is given in Ref [48].

The displacement field, as well as the non-homogeneity of the mechanical properties of the FGM plate, can be determined based on their nodal values. Therefore, the graded finite element method can be applied to achieve to effectively trace smooth variations of the material properties at the element level. Thus, the shape functions analogous to those of the displacement field can be expressed:

$$E = \sum_{i=1}^{8} E_i N_i, \quad \mathbb{N} = \begin{bmatrix} N_1 \dots N_8 \end{bmatrix}, \; \Xi = \begin{bmatrix} E_1 \dots E_8 \end{bmatrix}^T \tag{25}$$

in which $E_i$ is the modulus of elasticity for node i. $\mathbb{N}$ and $\boldsymbol{\Xi}$ are vectors of shape functions and modulus of elasticity of each element, respectively.

Hence, Equation (4) can be rewritten as:

$$\boldsymbol{D} = \Phi \mathbb{N} \Xi \tag{26}$$

The principle of virtual work could be used to achieve governing equations, which is defined as:

$$\delta \Pi = \delta U - \delta W = 0 \tag{27}$$

where:

$$\delta U = \int_V \delta \boldsymbol{\varepsilon}^T \boldsymbol{\sigma} dV \tag{28}$$

To extend the variation of strain energy, the definition of Green strain tensor and its variation are expressed as:

$$\boldsymbol{\varepsilon} = \boldsymbol{B}\ \Delta^{(e)},\ \ \delta\boldsymbol{\varepsilon} = \bar{\boldsymbol{B}}\ \delta\Delta^{(e)} \tag{29}$$

where B and $\bar{\boldsymbol{B}}$ in term of cylindrical and natural coordinates are as follow, respectively:

$$\begin{aligned} \boldsymbol{B} &= \boldsymbol{B}_L + \boldsymbol{B}_{NL} \\ \bar{\boldsymbol{B}} &= \boldsymbol{B}_L + \bar{\boldsymbol{B}}_{NL} \end{aligned} \tag{30}$$

$$\begin{aligned} \boldsymbol{B} &= \mathcal{B}_L + \mathcal{B}_{NL} \\ \bar{\boldsymbol{B}} &= \mathcal{B}_L + \bar{\mathcal{B}}_{NL} \end{aligned} \tag{31}$$

where:

$$\bar{B}_{NL} = \left(\bar{B}_{NL}^{(1)}\ \ \bar{B}_{NL}^{(2)}\ \ \bar{B}_{NL}^{(3)}\ \ \bar{B}_{NL}^{(4)}\ \ \bar{B}_{NL}^{(5)}\ \ \bar{B}_{NL}^{(6)}\ \ \bar{B}_{NL}^{(7)}\ \ \bar{B}_{NL}^{(8)}\right) \tag{32}$$

where $\overline{B_{NL}^{(i)}}.\ i = 1.2 \ldots .8$ and $\overline{B_{NL}}$ based on natural coordinates are noted in reference [48]. Therefore, Equation (27) can be written in a compact form as:

$$\boldsymbol{K}^{(e)}\Delta^{(e)} = \boldsymbol{F}^{Th(e)} \tag{33}$$

where:

$$K^{(e)} = \int_{V^{(e)}} \mathbb{N}\Xi\left(\mathcal{B}_{\mathrm{L}} + \overline{\mathcal{B}_{\mathrm{NL}}}\right)^T \Phi\left(\mathcal{B}_{\mathrm{L}} + \mathcal{B}_{\mathrm{NL}}\right)\mathrm{dV} = \int_{V^{(e)}} \mathbb{N}\Xi\mathcal{B}_{\mathrm{L}}^{\ T}\Phi\mathcal{B}_{\mathrm{L}}\mathrm{dV} +$$

$$\int_{V^{(e)}} \mathbb{N}\Xi\mathcal{B}_{\mathrm{L}}^{\ T}\Phi\mathcal{B}_{\mathrm{NL}}\mathrm{dV} + \int_{V^{(e)}} \mathbb{N}\Xi\overline{\mathcal{B}_{\mathrm{NL}}}^{T}\Phi\mathcal{B}_{\mathrm{L}}\mathrm{dV} + \int_{V^{(e)}} \mathbb{N}\Xi\overline{\mathcal{B}_{\mathrm{NL}}}^{T}\Phi\mathcal{B}_{\mathrm{NL}}\mathrm{dV} \tag{34}$$

$$F^{Th(e)} = \int_{V^{(e)}} \mathbb{N}\Xi\left(\mathcal{B}_{\mathrm{L}} + \overline{\mathcal{B}_{\mathrm{NL}}}\right)^T \Phi\varepsilon^{Th}\,\mathrm{dV} \tag{35}$$

and

$$dV = \frac{\beta^{(e)}h^{(e)}(b^{(e)} - a^{(e)})}{16}(\xi(b^{(e)} - a^{(e)}) + a^{(e)} + b^{(e)})d\xi\, d\eta\, d\zeta \tag{36}$$

The first term of the expanded form of the stiffness matrix is linear and is related to $K_L$, the second and third ones are nonlinear which are linearly dependent on the unknown variables and their summation is defined by $\boldsymbol{K}_{NL1}$. The fourth one is nonlinear which is the quadratic function of the unknown variables and is defined by $\boldsymbol{K}_{NL2}$.

By assembling the element matrices, the governing finite element equations of the FGM annular sector plate are:

$$\begin{aligned} &\boldsymbol{K}\ \Delta = \boldsymbol{F}, \\ &\boldsymbol{K}\ = \left(\boldsymbol{K}_{\ L} + \boldsymbol{K}_{\ NL1} + \boldsymbol{K}_{\ NL2}\right) \end{aligned} \tag{37}$$

The post-buckling behavior could be obtained with the gradually rising in used thermal load. There are the non-linear terms in the stiffness matrix, so an iterative technique must be applied. Newton–Raphson iterative procedure is employed to solve non-linear equilibrium equations [47]. The process at the n+1th iteration is as follows:

$$\Delta_{n+1} = \Delta_n + d\,\Delta_n \tag{38}$$

where:

$$d\,\Delta = \left(\boldsymbol{K}_{\boldsymbol{G}} + \boldsymbol{K}\right)^{-1}(\boldsymbol{F} - \boldsymbol{K}\,\Delta) \tag{39}$$

where $K_G$ can be computed as:

$$\boldsymbol{K}_{\boldsymbol{G}_{ij}} = \frac{\partial K_{im}}{\partial \Delta_j}\Delta_m \tag{40}$$

The sum of stiffness and geometric stiffness matrix $(K_G + K)$ is tangent stiffness matrix and can be expressed as follows:

$$\boldsymbol{K}^{\tan} = \boldsymbol{K}_{\ L} + 2\boldsymbol{K}_{\ NL1} + 3\boldsymbol{K}_{\ NL2} \tag{41}$$

Stages of the numerical solution of the problem may be summarized as follows;

1- The non-linear stiffness matrices (Eq. (34)) of the elements are determined based on the nodal displacements achieved at the previous loading increment. At the beginning of the solution procedure, these components are zero.

2- The overall stiffness and force matrices of the plate are constructed through assemblage of the stiffness and force matrices of the individual elements.

3- The boundary conditions are imposed.

4- The tangential stiffness matrix is established using Eq (41).

5- Eq. (39) is solved for determination of the required increments in the nodal displacements to reach the solution.

6- If the following convergence criterion is not met, the iterative solution has to be continued from step 1,

$$\frac{\left\|\Delta_{n+1} - \Delta_n\right\|}{\left\|\Delta_{n+1}\right\|} \cong \lambda \tag{42}$$

where $\lambda$ is a sufficiently small number, e.g., 0.0001.

7- In case of convergence occurrence, the results have to be saved (e.g., the load values and the resulting lateral deflections), the load is incremented and the solution process is continued from step 1.

8- Steps 1 to 7 are repeated till the assigned final values of the loads are reached.

In the present investigation, three various types of displacement boundary conditions are assumed as follow:

a) For annular sector plates with immovable simply supported edges:

$$\begin{aligned} &r=a,b:\ u,v,w=0,\\ &\theta=-\beta/2,\beta/2:\ u,v,w=0 \end{aligned} \tag{43}$$

b) For annular sector plates with immovable simply supported radial edges and free circumferential edges:

$$\theta=-\beta/2,\beta/2:\ u,v,w=0, \tag{44}$$

c) For annular sector plates with immovable simply supported circumferential edges and free radial edges:

$$r=a,b:\ u,v,w=0, \tag{45}$$

For simply supported edges condition, only the value of displacements at the mid-surface of the plate are equal to zero.

## 4. Results and Discussions

### *4.1. Validation*

In this part, a comparison study is carried out to show the effectiveness and accuracy of the present method. Thermal post-buckling of annular sector plates is not studied so far. Hence, post-buckling of an FGM square plate subjected to uniform temperature rise is re-considered [12] for verification purposes. Na and Kim [12] studied thermal post-buckling of all edges immovable simply supported FG plates subjected to uniform temperature rise using the three dimensional 18 node element. To convert the annular sector plate of the present study to a square plate, the sector angle is assumed as a small value $\beta = 0 \cdot 001$ rad and inner and outer radiuses of the plate are chosen as large values: a=200 m, b=200.2 m, and h=0.02. These geometric dimensions lead to nearly a square plate with length-to-thickness ratio of a/h=100. Furthermore, the material properties are assumed as $E_c = 393\ GPa.\ \alpha_c = 8.8 * 10^{-6}\ 1/℃$, $E_m = 199 \cdot 5\ GPa,\ \ \alpha_m = 13.3 * 10^{-6}\ 1/℃$ and $\upsilon = 0.3$ [12]. The post-buckling path of the center point of the plate for n=1 is achieved and compared with Ref [12]. Fig. 3. indicates the variations of temperature versus non-dimensional central displacement w/h. It can be seen that the present results are in an acceptable agreement with those reported in the literature.

### *4.2. Thermal Post-buckling Of FGM Annular Sector Plate*

In this section, the post-buckling analysis of all edges immovable simply supported FGM annular sector plates for different values of volume fraction index, sector angles, aspect ratio, and thickness ratio is presented. For this purpose, an FGM annular sector plate made of Al2O3-Ni with the following geometric and material properties characteristics is assumed:

a= 0.25, 0.5m, b=1m, h=0.025, 0.0125 m, $\beta = 60^\circ, 120^\circ, 240^\circ$.

$E_c = 393\,\text{GPa},\ \alpha_c = 8.8*10^{-6}\,1/℃$,

$E_m = 199.5\,\text{GPa}$, $\alpha_m = 13.3*10^{-6}\,1/℃$, $\upsilon = 0.3$.

Post-buckling paths are presented according to the non-dimensional transverse displacement $\frac{w}{h}$.. It should be noted that all the figures and contours are plotted by Matlab software. First, an immovable simply supported FGM annular sector plate is considered (a=0.5m, b=1m, h=0.025 m). The influence of power law exponents on the post-buckling paths of the plate subjected to uniform temperature rise is shown in Fig. 4. This result corresponds to an annular sector plate with $\beta = 60°$ and transverse displacement of the center point of the plate. Fig. 4. indicates that there is a sudden change in the load-deflection curve and the response of the plate can be introduced as a primary-secondary equilibrium path. Fig. 4. shows that for the homogeneous plate, the response of the plate is the bifurcation-type buckling, and the plate remains flat in the pre-buckling regions. Although, a non-linear stable equilibrium path is in the post-buckling area. FGM plates start to deflect immediately after the thermal load is applied. However, there is a sudden change in the load-deflection curve. The asymmetric distribution of the material properties in the thickness direction causes this behavior. The coupling between thermal forces and bending moments is created due to the asymmetric distribution of the material properties. In this case, the remained force passes through the mid-plane, not neutral surface of the plate. Hence, an extra bending moment influences on the plate, and the simply supported edges cannot tolerate the additional moments, and the plate starts to transverse displacement by initiation of applying the thermal load. For the cases that the movable simply supported FGM plates were subjected to in-plane normal loads [48], there is not any sudden change in the load-deflection curve. Also, the response of the plate could not be considered as a primary-secondary equilibrium path, and FGM plates show non-linear bending behavior with unique and stable equilibrium paths.

A comparison between [48] and present results denotes that in the present study when all edges of the plate are immovable (*u=v=w=0*), the behavior of the FGM plate subjected to thermal loads is considered as a primary-secondary equilibrium path. Also, results show that by increasing the power law exponent, the volume

fraction of ceramic constituent causes decreases, and hence, the plate becomes softer and experiences more transverse displacement. Moreover, by increasing the power law exponent, the strength of the plate decreases at the post-buckling region. Figs. 5 a-c show the deflection of the plate for different temperatures and n=1, z=h/2.

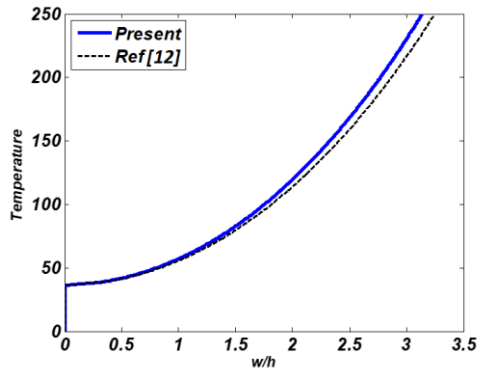


**Fig. 3.** A comparison between post-buckling equilibrium curves obtained by the present 3D elasticity procedure and Ref [12] for immovable simply supported FGM square plate subjected to uniform temperature rise ($r = \frac{a+b}{2}.\theta = 0$. z=h/2).

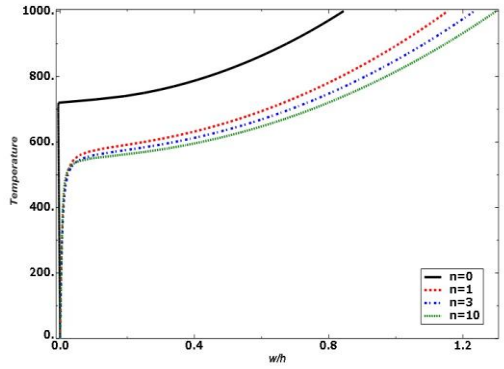


**Fig. 4.** Influence of different power law exponent on post-buckling curves of annular sector plate made of FGM with immovable simply supported edges (h=0.025 m and $\beta = 60°$)

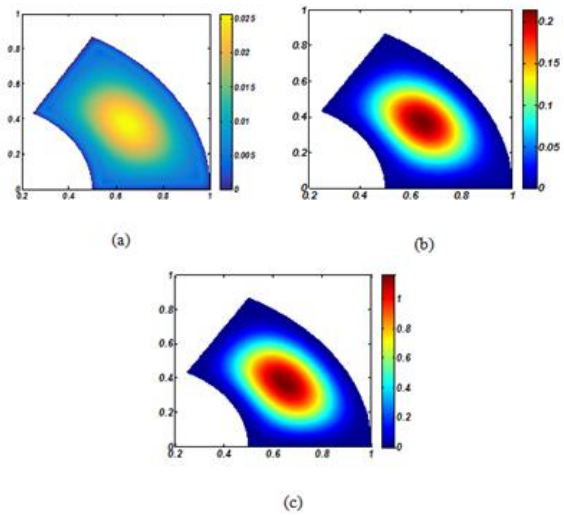


**Fig. 5.** The post-buckling deformation type of annular sector plate made of FGM with immovable simply supported edges for (n=1, z=h/2), (h=0.025 m and $\beta = 60°$) a) T=520°C, b) T=600 °C, c) T=1000°C

The influence of thickness ratio on post-buckling paths of all-edge-immovable simply supported FGM annular sector plate subjected to uniform temperature rise is also studied. Therefore, the thickness of the plate is considered to be h=0.0125 m. Fig. 6 indicates post-buckling paths of the center point of the plate with $\beta = 60°$ for various power law exponent. A comparison between Figs. 4. and 6. demonstrates that by decreasing the thickness of the plate, the strength of the plate at the buckling and post-buckling region is decreased and the plate experiences more lateral deflection. Figs. 7 a-c shows the deflection of the plate for different temperatures and for n=1, z=h/2.

In order to study the influence of sector angle on thermal post-buckling behavior of plate, an immovable simply supported FGM annular sector plate with $\beta = 120°, 240°$ is considered. Influence of power law exponents on center point deflection of the plate with $\beta = 120°, 240°$ is shown in Figs. 8. and 9., respectively. A comparison between results of $\beta = 120°, 240°$ and $\beta = 60°$indicate that by increasing the sector angle, the strength of plate at buckling and post-buckling areas is decreased and the plate experiences more lateral deflection. Figs. 10 a-c and Figs. 11 a-c show the deflection of the plate for different temperatures with $\beta = 120°, 240°$ , respectively (n=1, z=h/2). These results indicate that by increasing the temperature in the deep post-buckling regime, higher mode shapes are appeared. Also, these figures denote that, by increasing the sector angle, the number of buckling waves is increased.

The influence of aspect ratio on post-buckling paths of all-edge-immovable simply supported FGM annular sector plate subjected to uniform temperature rise is also studied. Therefore, the inner radius of the plate is supposed to be a=0.25 m (b=1 m, h=0.025 m, $\beta = 60°$)). Fig. 12. indicates post-buckling paths of the center point of the plate with different power law exponent. A comparison between Figs. 4 and 12 demonstrates that by decreasing the inner radius of the plate, the strength of the plate at buckling and post-buckling areas is decreased. Figs. 13. a-c shows the deflection of the plate for different temperatures through the post-buckling path and for n=1, z=h/2.

Now, the influences of various boundary conditions on thermal post-buckling of FGM annular sector plate subjected to uniform temperature rise have been investigated (a=0.5 m, b=1 m, h=0.025 m, $\beta = 60°$). The influence of power law exponents on the center point deflection of FG annular sector plate with immovable simply supported radial edges and free circumferential edges is shown in Fig. 14. It can be seen that the post-buckling response of

the FGM plate can be considered as a primary-secondary equilibrium path with a stable post-buckling regime. By applying the free edges condition, the strength of the plate at post-buckling is noticeably decreased. Figs. 15. a-c shows deflection of the plate for different temperatures through the equilibrium path for n=1, z=h/2.

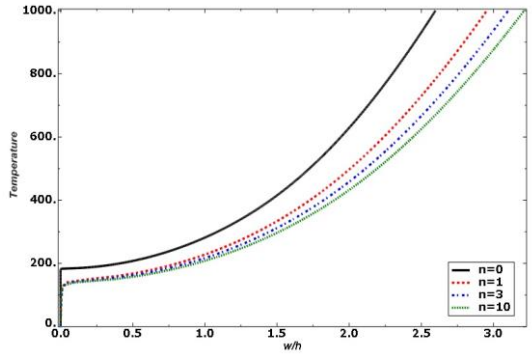


**Fig. 6.** Influence of different power law exponent on post-buckling curves of annular sector plate made of FGM with immovable simply supported edges (h=0.0125 m and $\beta$ = 60°)

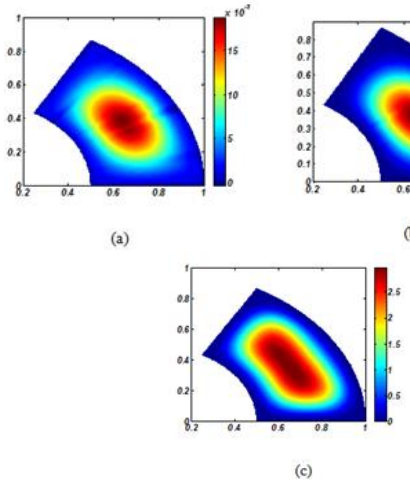


**Fig. 7.** The post-buckling deformation type of annular sector plate made of FGM with immovable simply supported edges for (n=1, z=h/2), (h=0.0125 m and $\beta$ = 60°), a) T=120℃, b) T=180 ℃, c) T=1000℃

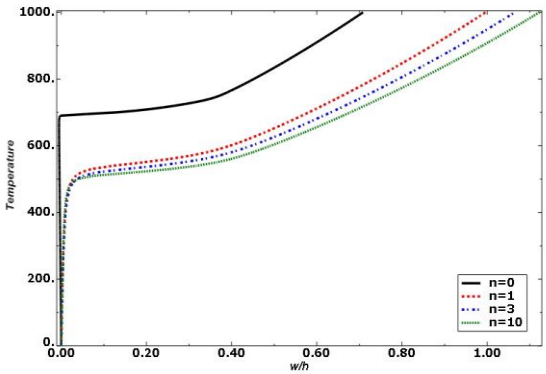


**Fig. 8.** Influence of different power law exponent on post-buckling curves of annular sector plate made of FGM with immovable simply supported edges (h=0.025 m and $\beta$ = 120°)

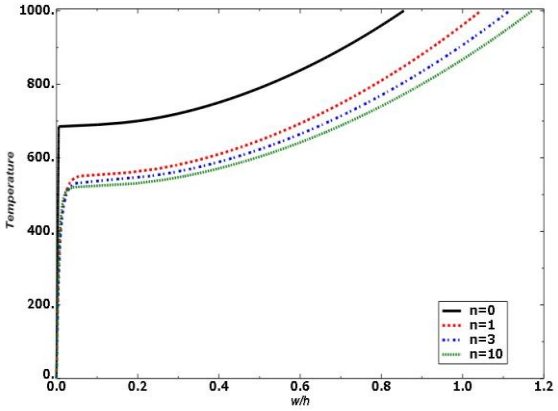


**Fig. 9.** Influence of different power law exponent on post-buckling curves of annular sector plate made of FGM with immovable simply supported edges (h=0.025 m and $\beta$ = 240°)

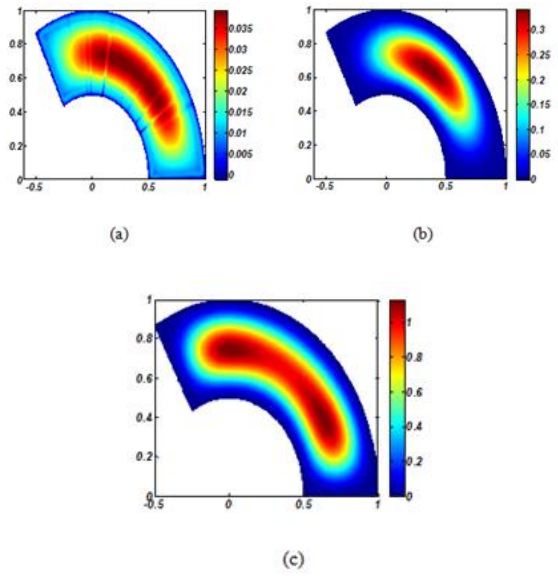


**Fig. 10.** The post- buckling deformation type of annular sector plate made of FGM with immovable simply supported edges for (n=1, z=h/2), (h=0.025 m and $\beta$ = 120°)), a) T=480℃, b) T=580 ℃, c) T=1000℃

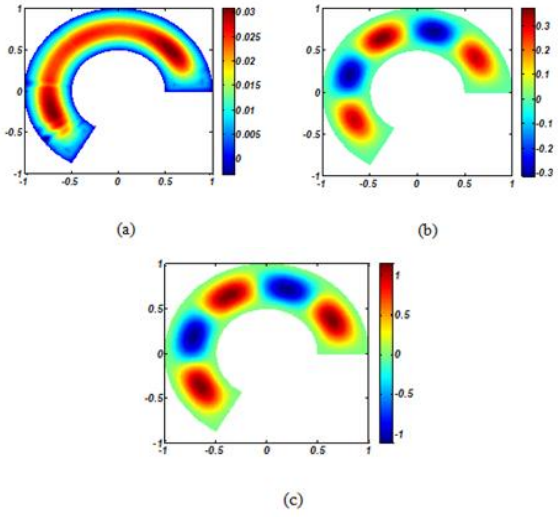


**Fig. 11.** The post- buckling deformation type of annular sector plate made of FGM with immovable simply supported edges

for (n=1, z=h/2), (h=0.025 m and $\beta = 240°$)), a) T=510℃, b) T=610 ℃, c) T=1000℃

Post-buckling paths of FGM plate with immovable circumferential edges and free radial edges with various power law exponent are shown in Fig. 16. The influence of power law exponent on post-buckling paths is similar to the other boundary conditions. But by comparing the results of various boundary conditions, it is shown that in this case, the buckling and post-buckling of the plate are increased. Figs. 17. a-c shows deflection of the plate for different temperatures through the equilibrium path for n=1, z=h/2. Finally, for giving a clear sense of the benchmark results, the critical temperature values of the presented curves extracted from post-buckling paths are reported in Table 1.

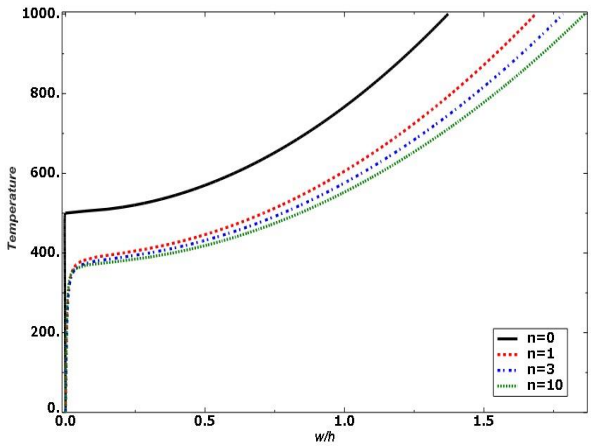


**Fig. 12.** Influence of different power law exponent on post-buckling curves of annular sector plate made of FGM with immovable simply supported edges (a=0.25, h=0.025 m and $\beta = 60°$)

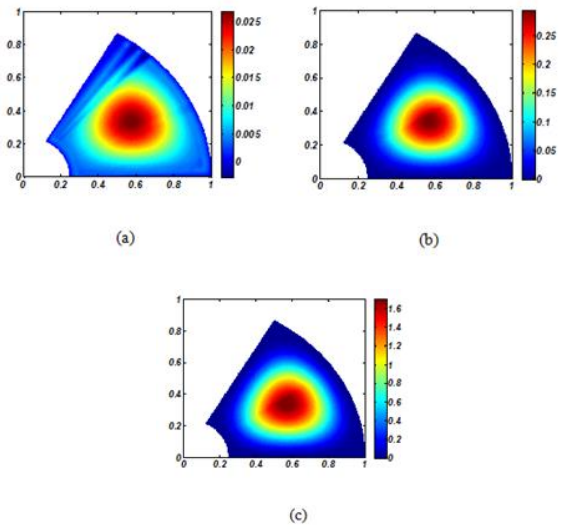


**Fig. 13.** The post- buckling deformation type of annular sector plate made of FGM with immovable simply supported edges for (n=1, z=h/2), (a=0.25, h=0.025 m and $\beta = 60°$), a) T=360℃, b) T=410 ℃, c) T=1000℃

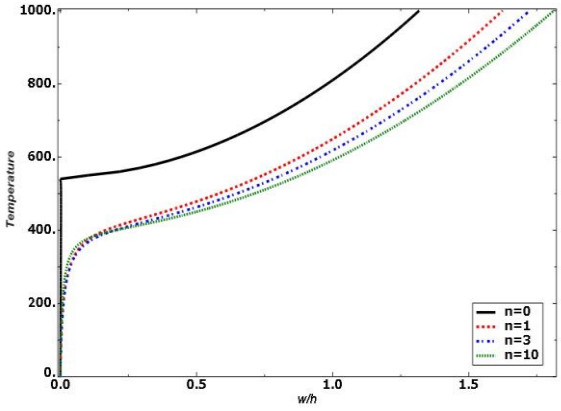


**Fig. 14.** Influence of different power law exponent on post-buckling curves of annular sector plate made of FGM with immovable simply supported edges at $\theta = -\frac{\beta}{2}.\frac{\beta}{2}$ for different power law exponent (a=0.5 m, h=0.025 m and $\beta = 60°$)

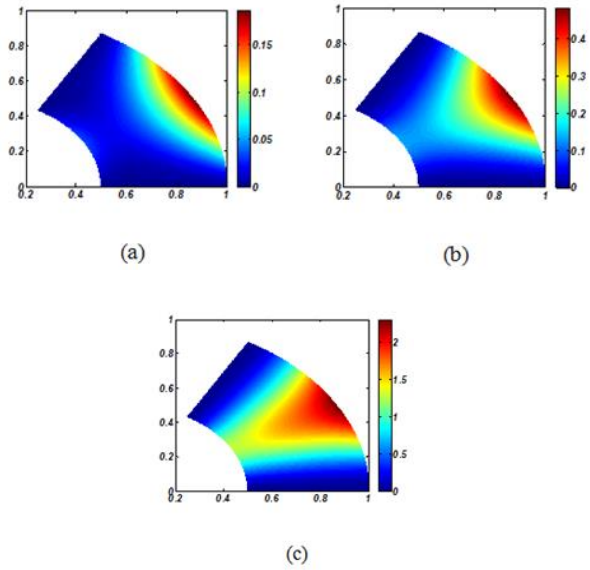


**Fig. 15.** The post-buckling deformation type of annular sector plate made of FGM with immovable simply supported edges at $\theta = -\frac{\beta}{2}.\frac{\beta}{2}$ for (n=1, z=h/2), (h=0.025 m and $\beta = 60°$), a) T=310℃, b) T=410 ℃, c) T=1000℃

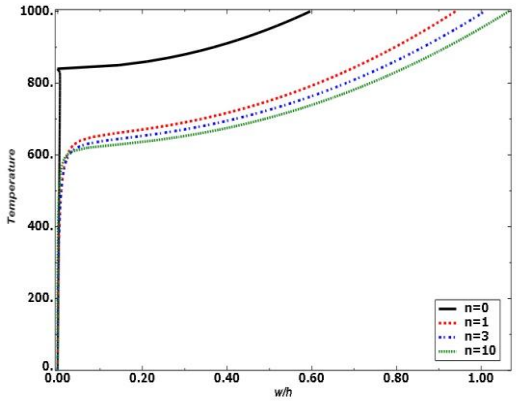


**Fig. 16.** Influence of different power law exponent on post-buckling curves of annular sector plate made of FGM with immovable circumferential edges and free radial edges (a=0.5 m, h=0.025 m and $\beta = 60°$)

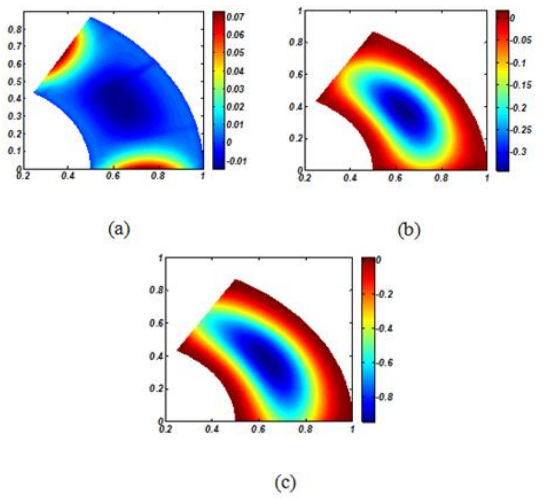


**Fig. 17.** The post- buckling deformation type of annular sector plate made of FGM with immovable simply supported edges at r=a, b for (n=1, z=h/2), (h=0.025 m and $\beta = 60°$), a) T=560℃, b) T=700 ℃, c) T=1000℃

**Table 1.** The Influence of different power law exponent on critical temperature of immovable simply supported FGM annular sector plates

| N | a=0.5m, b=1m h=0.025 m $\beta = 60°$ | a=0.5m, b=1m h=0.0125 m $\beta = 60°$ | a=0.5m, b=1m h=0.025 m $\beta = 120°$ | a=0.25, b=1m h=0.025 m $\beta = 60°$ |
|---|---|---|---|---|
| n=0 | 714.54 | 186.703 | 689.923 | 503.226 |
| n=1 | 538.412 | 136.084 | 507.203 | 369.194 |
| n=3 | 535.814 | 133.0929 | 505.518 | 366.82 |
| n=10 | 533.221 | 130.0932 | 501.139 | 362.977 |

## 5. Conclusions

In this study, the 3D elasticity approach is used to investigate the thermal post-buckling analysis of functionally graded annular sector plates. The Green-Lagrange nonlinear strain-displacement relation is assumed for large deflections. The governing equations are extended via the principle of virtual work and solved based on a GFEM. Finally, Newton–Raphson procedure is applied to solve the non-linear equilibrium equations. The influences of material gradient exponent, various sector angles, thickness ratio, aspect ratio, and three various boundary conditions on the thermal post-buckling response of FGM annular sector plates have been carried out.

Some of the innovations in the present study are:

- Analyzing post-buckling of FGM annular sector plates subjected to uniform temperature rise for the first time.
- Using 3D elasticity theory instead of the approximate plate theories that shows the behavior of the plate more real.
- The Green-Lagrange nonlinear strain-displacement relation is taken into account for large deflections.
- The coupling between thermal load and bending moments of FGM is studied.
- The influences of three various boundary conditions on the post-bucking response of plate have been presented.

Furthermore, the following conclusions are obtained from the results:

- The post-buckling behavior of the FGM annular sector plate for different boundary conditions can be noticed as primary-secondary equilibrium path.
- While the power law exponent increases, the post-buckling resistance of the plate is decreased.
- By increasing the sector angle, the post-buckling strength of the plate decreases and higher mode shapes appears in the deep post-buckling regime.
- While the thickness of the plate decreases, the post-buckling strength of the plate is noticeably decreased.
- The post-buckling strength of the plate with immovable circumferential edges is much more than the other boundary conditions.

## References

[1] Ghannadpour, Ovesy, S. H. and Nassirnia, M., 2012. Buckling analysis of functionally graded plates under thermal loadings using the finite strip method. Computers & structures, 108, pp. 93-99.

[2] Mansouri, M. and Shariyat, M., 2014. Thermal buckling predictions of three types of high-order theories for the heterogeneous orthotropic plates, using the new version of DQM. Composite Structures, 113, pp. 40-55.

[3] Soleimanian, S., Davar, A., Eskandari Jam, J., Zamani, M. R., and Heydari Beni, M., 2020. Thermal Buckling and Thermal Induced free Vibration Analysis of Perforated Composite Plates: a Mathematical Model. Mechanics of Advanced Composite Structures, 7(1), pp.15-23.

[4] Kiarasi, F., Babaei, M., Dimitri, R., and Tornabene, F. R., 2020. Hygrothermal modeling of the buckling behavior of sandwich plates with nanocomposite face sheets resting on a Pasternak foundation. Continuum Mechanics and Thermodynamics, pp.1-22.

[5] Shariat, B. S., Eslami, M., and Bagri, A., 2006. Thermoplastic Stability of Imperfect Functionally Graded Plates Based on the Third Order Shear Deformation Theory. in Engineering Systems Design and Analysis. 42487, pp. 313-319.

[6] Shariat, B. S. and Eslami, M., 2007. Buckling of thick functionally graded plates under mechanical and thermal loads. Composite Structures, 78(3), pp. 433-439.
[7] Duc, N. D., and Tung, H., 2010. Mechanical and thermal post buckling of shear-deformable FGM plates with temperature-dependent properties. Mechanics of Composite Materials, 46(5), pp. 461-476.
[8] Duc, N. D., and Van Tung, H., 2011. Mechanical and thermal post buckling of higher order shear deformable functionally graded plates on elastic foundations. Composite Structures, 9(11), pp. 2874-2881.
[9] Lal, A., Jagtap, K., and Singh, B., 2013. Post buckling response of functionally graded materials plate subjected to mechanical and thermal loadings with random material properties. Applied Mathematical Modelling, 37(5), pp. 2900-2920.
[10] Lee, Y., Zhao, X., and Reddy, J., 2010. Post buckling analysis of functionally graded plates subject to compressive and thermal loads. Computer Methods in Applied Mechanics and Engineering, 199(25-28), pp. 1645-1653.
[11] Liew, K., Yang, J., and Kitipornchai, S., 2003. Post buckling of piezoelectric FGM plates subject to thermo-electro-mechanical loading. International Journal of Solids and Structures, 40, (15), pp. 3869-3892.
[12] Na, K. S., and Kim, J. H., 2006. Thermal post buckling investigations of functionally graded plates using 3-D finite element method. Finite Elements in Analysis and Design, 42(8-9), pp. 749-756.
[13] Shen, H. S., 2005. Postbuckling of FGM plates with piezoelectric actuators under thermo-electro-mechanical loadings. International Journal of Solids and Structures, 42(23), pp. 6101-6121.
[14] Van Tung, H., and Duc, N. D., 2010. Nonlinear analysis of stability for functionally graded plates under mechanical and thermal loads. Composite Structures, 92(5), pp. 1184-1191.
[15] Woo, J., Meguid, S., Stranart, J., and Liew, K., 2005. Thermomechanical post-buckling analysis of moderately thick functionally graded plates and shallow shells. International Journal of Mechanical Sciences, 7(8), pp. 1147-1171.
[16] Yang J. and Shen, H. S., 2003. Nonlinear bending analysis of shear deformable functionally graded plates subjected to thermo-mechanical loads under various boundary conditions. Composites Part B: Engineering, 34(2), pp. 103-115.
[17] Zhu, P., Zhang, L., and Liew, K., 2014. Geometrically nonlinear thermomechanical analysis of moderately thick functionally graded plates using a local Petrov–Galerkin approach with moving Kriging interpolation. Composite Structures, 107, pp. 298-314.
[18] Ghiasian, S., Kiani, Y., Sadighi, M., and Eslami, M., 2014. Thermal buckling of shear deformable temperature dependent circular/annular FGM plates. International Journal of Mechanical Sciences, 81, pp. 137-148.
[19] Jalali, S., Naei, M., and Poorsolhjouy, A., 2010. Thermal stability analysis of circular functionally graded sandwich plates of variable thickness using pseudo-spectral method. Materials & Design, 31(10), pp. 4755-4763.
[20] Kiani, Y., and Eslami, M.,2013. An exact solution for thermal buckling of annular FGM plates on an elastic medium. Composites Part B: Engineering, 45(1), pp. 101-110.
[21] Kiani, Y., and Eslami, M., 2013. Instability of heated circular FGM plates on a partial Winkler-type foundation. Acta Mechanica, 224(5), pp. 1045-1060.
[22] Najafizadeh, M., and Eslami, M., 2002. First-order-theory-based thermoelastic stability of functionally graded material circular plates. AIAA Journal, 40(7), pp. 1444-1450.
[23] Najafizadeh, M., and Hedayati, B., 2004. Refined theory for thermoelastic stability of functionally graded circular plates. Journal of thermal stresses, 27(9), pp. 857-880.
[24] Najafizadeh, M., and Haidari, H., 2004. Thermal buckling of functionally graded circular plates based on higher order shear deformation plate theory. European Journal of Mechanics-A/Solids, 23(6), pp. 1085-1100.
[25] Prakash, T., and Ganapathi, M., 2006.Asymmetric flexural vibration and thermoelastic stability of FGM circular plates using finite element method. Composites Part B: Engineering, 37(7-8), pp. 642-649.
[26] Aghelinejad, M., Zare, K., Ebrahimi, F., and Rastgoo, A., 2011. Nonlinear thermomechanical post-buckling analysis of thin functionally graded annular plates based on Von-Karman's plate theory. Mechanics of Advanced Materials and Structures, 18(5), pp. 319-326.
[27] Fallah, F., and Nosier, A., 2012. Nonlinear Bending and Post Buckling of Functionally Graded Circular Plates under Asymmetric Thermo-Mechanical Loading. in Materials with Complex Behaviour II: Springer, pp. 383-417.
[28] Kadam, P., and Panda, S., 2014. Nonlinear analysis of an imperfect radially graded annular plate with a heated edge. International Journal of Mechanics and

Materials in Design, vol. 10, no. 3, pp. 281-304.

[29] Kiani, Y., and Eslami, M., 2014. Thermal post-buckling of imperfect circular FGM plates: examination of Voigt, Mori-tanaka and self-consistent schemes. Journal of Pressure Vessel Technology.

[30] Li, S. R., Zhang, J. H., and Zhao, Y. G., 2007. Nonlinear thermomechanical post-buckling of circular FGM plate with geometric imperfection. Thin-Walled Structures, 45(5), pp. 528-536.

[31] Ma, L., and Wang, T., 2003.Nonlinear bending and post-buckling of a functionally graded circular plate under mechanical and thermal loadings. International Journal of Solids and Structures, 40, (13-14), pp. 3311-3330.

[32] Sepahi, O., Forouzan, M., and Malekzadeh, P., 2011. Thermal buckling and post buckling analysis of functionally graded annular plates with temperature-dependent material properties. Materials & Design, 32 (7), pp. 4030-4041.

[33] Hosseini-Hashemi, S., Akhavan, H., Taher, H. R. D., Daemi, N., and Alibeigloo, A., 2010.Differential quadrature analysis of functionally graded circular and annular sector plates on elastic foundation. Materials & Design, 31(4), pp. 1871-1880.

[34] Naderi, A., and Saidi, A., 2011. Exact solution for stability analysis of moderately thick functionally graded sector plates on elastic foundation. Composite Structures, 93(2), pp. 629-638.

[35] Naderi, A., and Saidi, A., 2011. An analytical solution for buckling of moderately thick functionally graded sector and annular sector plates. Archive of Applied Mechanics, 81(6), pp. 809-828.

[36] Naderi, A., and Saidi, A., 2011.Buckling analysis of functionally graded annular sector plates resting on elastic foundations. Proceedings of the Institution of Mechanical Engineers, Part C: Journal of Mechanical Engineering Science, 225, (2), pp. 312-325.

[37] Asemi, K., Salehi, M., and Akhlaghi, M., 2014. Three dimensional biaxial buckling analysis of functionally graded annular sector plate fully or partially supported on Winkler elastic foundation. Aerospace Science and Technology, 39, pp. 426-441.

[38] Asemi, K., Salehi, M., and Akhlaghi, M., 2015. Three dimensional graded finite element elasticity shear buckling analysis of FGM annular sector plates. Aerospace Science and Technology, 43, pp. 1-13.

[39] Saidi, A., and Baferani, A. H., 2010. Thermal buckling analysis of moderately thick functionally graded annular sector plates. Composite Structures, 92(7), pp. 1744-1752.

[40] Jabbarzadeh, M., and Baghdar Delgosha, M., 2013. Thermal buckling analysis of FGM sector plates using differential quadrature method. Modares Mechanical Engineering, 13( 2), pp. 33-45.

[41] Shaterzadeh, A. R., Abolghasemi, S., & Rezaei, R. 2014. Finite element analysis of thermal buckling of rectangular laminated composite plates with circular cut-out. Journal of thermal stresses, 37, (5), 604-623.

[42] Abolghasemi, S., Shaterzadeh, A. R., & Rezaei, R. 2014. Thermo-mechanical buckling analysis of functionally graded plates with an elliptic cutout. Aerospace Science and Technology, 39, 250-259.

[43] Shaterzadeh, A. R., Rezaei, R., & Abolghasemi, S. 2015. Thermal buckling analysis of perforated functionally graded plates. Journal of Thermal Stresses, 38(11), 1248-1266.

[44] Shariyat, M., Behzad, H., and Shaterzadeh, A. R. 2018. 3D thermomechanical buckling analysis of perforated annular sector plates with multiaxial material heterogeneities based on curved B-spline elements. Composite Structures, 188, pp.89-103.

[45] Behzad, H., Shaterzadeh, A., and Shariyat, M., 2017. Thermal buckling analysis of functionally graded perforated annular sector plates using 3D elasticity theory. Journal of Thermal Stresses, 40(12), pp. 1545-1562, .

[46] Shaterzadeh, A., Behzad, H., and Shariyat M.,, 2018. Stability analysis of composite perforated annular sector plates under thermomechanical loading by finite element method. International Journal of Structural Stability and Dynamics, 18(07), pp. 1850100.

[47] Zienkiewicz, O. C., and Taylor, R. L., 2005. The finite element method: its basis and fundamentals. 6th edition, Butterworth-Heinemann .

[48] Asemi, K., Salehi, M., Akhlaghi, M., 2014 . Post-buckling analysis of FGM annular sector plates based on three dimensional elasticity graded finite elements. International Journal of Non-Linear Mechanics, 67, pp. 164-177.